

The role of carbon for superconductivity in MgC_xNi_3 from specific heat

A. Wälte,* G. Fuchs, K.-H. Müller, S.-L. Drechsler, K. Nenkov, and L. Schultz

Leibniz-Institut für Festkörper- und Werkstoffforschung Dresden, Postfach 270116, D-01171 Dresden, Germany

(Dated: 8th December 2018)

The influence of carbon deficiency on superconductivity of MgCNi_3 is investigated by specific heat measurements in the normal and superconducting state. In order to perform a detailed analysis of the normal state specific heat, a computer code is developed which allows for an instantaneous estimate of the main features of the lattice dynamics. By analyzing the evolution of the lattice vibrations within the series and simultaneously considering the visible mass enhancement, the loss in the electron-phonon coupling can be attributed to significant changes of the prominent Ni vibrations. The present data well supports the recently established picture of strong electron-phonon coupling and ferromagnetic spin fluctuations in this compound.

PACS numbers: 74.25.Bt, 74.25.Kc, 75.40.Cx

The discovery of superconductivity in MgCNi_3 has caused much attention,¹ since the large Ni content suggests a magnetic state rather than superconductivity. Indeed, up to now a lot of experimental and theoretical publications point to a ferromagnetic instability at temperatures near and below the superconducting transition temperature $T_c \approx 7$ K.^{2,3,4,5,6} So far there is much discussion on the carbon content in MgCNi_3 , since only samples with carbon excess of ≈ 50 % show large T_c values, whereas for the stoichiometric composition a strongly reduced T_c is found,^{7,8} which may be triggered by enhanced pair-breaking due to increasing spin fluctuations.⁹ However specific heat measurements indicate that this is not the case but instead the electron-phonon coupling is significantly reduced,⁵ accompanied by a considerable hardening of low-energy vibrations.¹⁰ Band structure calculations predict a constant⁹ or decreasing⁵ electron density of states at the Fermi level (EDOS), leaving the interesting prospect of significantly changing lattice dynamics. Recent measurements of the carbon isotope effect support this picture.¹¹

Polycrystalline samples of MgCNi_3 have been prepared by solid-state reaction. The high volatility of Mg was balanced in the usual way by Mg excess. Three samples of nominal composition $\text{Mg}_{1.2}\text{C}_{x_n}\text{Ni}_3$ with $x_n = 0.75, 0.85$ and 1.00 (n =nominal) have been prepared. For comparison the previously reported sample with $x_n = 1.60$ and $T_c = 6.8$ K is chosen.⁶ Details on the preparation procedure have been published elsewhere.¹ The obtained samples were characterized by x-ray diffractometry. Due to the relatively low carbon content no additional graphite was found in the samples, instead a small fraction of MgNi_2 forms with decreasing carbon content. However the fraction never exceeds 6 Vol.-% and has minor influence on the following specific heat analysis. The positions of the reflexes in the x-ray diffractograms are shifted to higher angles for decreasing carbon content. The left panel of Fig. 1 shows a magnification of the region $2\Theta \approx 84$ deg, where the influence of the carbon deficiency is visible. For a full diffractogram of the $x_n = 1.60$ sample see Ref. 6. The lattice constants of the samples were determined using the Rietveld code FULLPROF.¹² From that

the effective carbon content was estimated according to Ref. 7. The dependence is plotted in the right panel of Fig. 1 together with the estimated superconducting transition temperatures.⁷ It is obvious that the present samples with $x_n \leq 1.00$ are multi-phase samples. However this is of minor importance for the following analysis. The specific heat was measured for $T = 2 - 300$ K and magnetic fields up to $\mu_0 H = 12$ T using a Quantum Design Physical Property Measurement System. For the sample with $x_n = 1.00$, which shows a considerably broadened superconducting transition (due to its multi-phase nature) the measurement was extended down to $T = 0.3$ K.

I. COMPUTATIONAL DETAILS

From the mathematical point of view, the extraction of the phonon density of states (PDOS) from specific heat measurements is ill-posed. This means, that a number of very different PDOS can lead to very similar specific heat curves. From the experimental point of view one has to extract the phonon specific heat from the electron and other non-phononic background exactly. In reality temperature dependent effects (e.g. softening) then prevent an inversion approach in most cases. From this starting point we developed a computer code based on simple models, namely a Debye and an Einstein model, in order to get a rough estimate on the lattice dynamics from specific heat measurements instead of a mathematical exact inversion. Specifications of the code, which is fully based on ROOT,¹³ will be published elsewhere. Here we want to sketch only the main ideas and illustrate the capabilities of the code. The specific heat of a compound with n atoms per unit cell has $3n - 3$ optical and 3 acoustic vibrations which can be approximated by a linear combination of Einstein and Debye models. The contribution of the Einstein phonons to the specific heat is given by:

$$c_E(T) = \sum_{i=3}^N R \left(\frac{\Theta_{Ei}}{T} \right)^2 \frac{\exp(\Theta_{Ei}/T)}{[\exp(\Theta_{Ei}/T) - 1]^2},$$

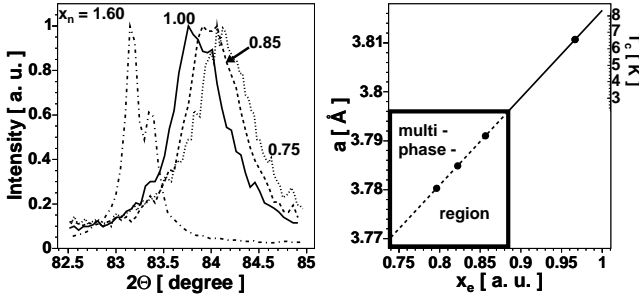


Figure 1: Structural influence of nominal carbon content on MgC_xNi_3 . Left panel: x-ray diffractogram around $2\Theta \approx 84$ deg. Right panel: relation between lattice constant a , effective carbon content x_e and T_c according to Ref. 7 for the investigated samples.

with number of optical modes N and Einstein temperatures Θ_{Ei} . The Debye contribution reads:

$$c_D(T) = \sum_{i=0}^2 3R \left(\frac{T}{\Theta_{Di}} \right)^3 \int_0^{\Theta_{Di}/T} dx \frac{e^x x^4}{(e^x - 1)^2},$$

with Debye temperatures Θ_{Di} . The form of the phonon density of states is thereby simplified as:

$$F(\omega) = 3R\omega^2 \sum_{i=0}^2 \frac{\theta(\omega_{Di} - \omega)}{\omega_{Di}^3} + \sum_{i=3}^N \frac{\exp\left[-\frac{(\omega - \omega_{Ei})^2}{2\sigma_i^2}\right]}{\sigma_i \sqrt{2\pi}},$$

with step function $\theta(x_0 - x)$ and the characteristic temperatures in meV, indicated by ω_{Di} and ω_{Ei} . For the case of MgCNi_3 one is left with 3 Debye and 12 Einstein terms, adding up to 15 parameters. To avoid the need of restrictions on the parameters we developed a fast converging algorithm. It makes use of a library containing integrated values of a single Debye and Einstein model for $\Delta T = 1$ K temperature intervals between $T = 2$ K and 300 K and the overall integral of the two models in the interval $T = 2 - 300$ K. The algorithm integrates the measured specific heat in a number of temperature intervals and once over the measurement range $T = 2 - 300$ K. The use of the overall integral for the fitting procedure accelerates the procedure considerably and most importantly allows the omission of parameter-restrictions. The code was statistically tested by randomly distributing 6 Einstein and 2 Debye terms. The fitting result was then compared to the starting conditions. Fig. 2 shows the resulting energy resolution gained from 20000 analyzed specific heat model-curves. This test shows that the energy resolution is weak for low-energy optical and high-energy acoustic vibrations, which are both rare cases. However, there is still potential in the algorithm to improve the energy resolution. For example by using a set of weighting factors for different temperature regions, which we are currently working on.

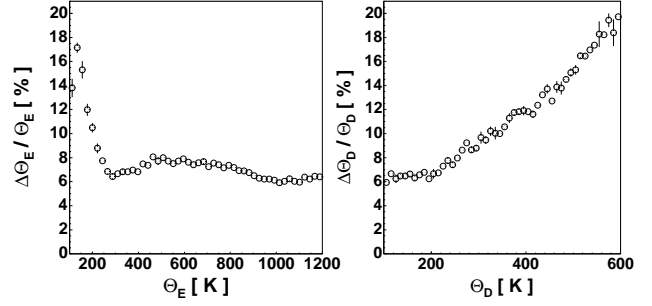


Figure 2: Energy resolution $\Delta\Theta_{Di}/\Theta_{Di}$ and $\Delta\Theta_{Ei}/\Theta_{Ei}$ of the code in a background of 6 (5) random Einstein and 1 (2) random Debye terms. Left panel: energy resolution for one Einstein vibration. Right panel: energy resolution for one Debye vibration.

II. ANALYSIS AND DISCUSSION

The specific heat of the sample with $x_n = 1.00$ is shown in Fig. 3 (the samples with $x_n = 0.85$ and 0.75 show very similar results and are omitted for clarity). The specific heat of MgCNi_3 is given by a lattice part $c_{\text{lattice}}(T)$, determined by the above mentioned code and an electron part $\gamma_N T$ with the Sommerfeld parameter:

$$\gamma_N = [1 + \lambda_{\text{ph}} + \lambda_{\text{sf}}(0)] \gamma_0, \quad (1)$$

with free electron parameter $\gamma_0 = 11$ mJ/(molK²). The mass enhancement due to the electron-paramagnon coupling can be estimated from

$$\lambda_{\text{sf}}(T) = \frac{6}{\pi k_B T} \int_0^\infty d\omega \alpha^2 F_{\text{sf}}(\omega) \left\{ -z - 2z^2 \Im[\psi'(iz)] - z^3 \Re[\psi''(iz)] \right\}, \quad (2)$$

where $\psi(iz)$ is the digamma function and $z = \omega/(2\pi k_B T)$. The electron-paramagnon spectral density is given by

$$\alpha^2 F_{\text{sf}}(\omega) = a\omega\theta(\omega_{\text{sf}} - \omega) + \frac{b}{\omega^3}\theta(\omega - \omega_{\text{sf}}).$$

The paramagnon energy, which was estimated in the case of $x_n = 1.60$ as $\omega_{\text{sf}} \approx 2.15$ meV,⁶ was also used for the present samples. The black line in Fig. 3 is the result of the fitting procedure. The differences between the data and fit results are shown in the inset for $x_n = 0.75$, 0.85 and 1.00 . They are very small, in particular for $x_n = 0.85$ and 1.00 , indicating the success of the fitting procedure.

Fig. 4 shows the low temperature region of the specific heat. The reduction of γ_N and the increasing flattening of the curves with decreasing carbon content was already discovered in a previous work by Shan et al.⁵ For $x_n = 1.00$ a strongly broadened superconducting transition is visible at $T_c \approx 2.5$ K, in accord with the mentioned multi-phase nature. The deviation from the low temperature Debye approximation (linear behavior) due to spin fluctuations is clearly seen for all samples (Fig. 4).

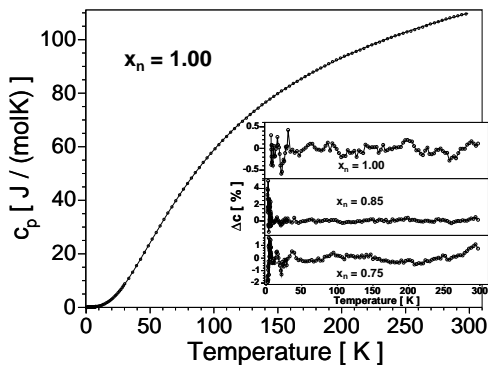


Figure 3: Specific heat of $\text{MgC}_{1.00}\text{Ni}_3$. Solid line: specific heat fit (see text for details). Inset: relative difference between fit and specific heat for $x_n = 1.00$, 0.85 and 0.75 (from top to bottom).

The model description of the normal state is given as solid lines. For $x_n = 1.00$ the conservation of entropy of the superconducting state, which is expected for a phase transition of second order, was used as an additional requirement for a successful fit (inset of Fig. 4). γ_N was varied with a step-size of 0.05 mJ/molK^2 until the relative difference shown in the inset of Fig. 4 was minimized. Close to the final value of γ_N , the derived sets of vibrational parameters did not appear qualitatively different from each other. The results of the fitting procedure are summarized in Tab. I. The electron-paramagnon coupling constant $\lambda_{\text{sf}}(0)$ only slightly decreases by lowering the carbon content, despite a predicted increase of spin fluctuations.⁹ The electron-phonon coupling constant shows a strong decrease from $\lambda_{\text{ph}} = 1.84$ ($x_n = 1.60$) down to $\lambda_{\text{ph}} = 1.06$ ($x_n = 0.75$), in agreement with results obtained by Shan et al.⁵

Fig. 5 shows the resulting phonon density of states, $F(\omega)$ for $x_n = 0.75$, 0.85 and 1.00 in comparison with previous results for $x_n = 1.60$.⁶ There are two main changes visible within the series. First there is a considerable change of the high-energy mode, which is expected, since it is dominated by carbon. Second all low-energy modes are slightly shifted to higher energies, accompanied by the shrinking of the unit cell. The extent of this behavior can be quantified by calculating the characteristic phonon frequency:

$$\omega_{\text{ln}} = \exp \left[\frac{2}{\lambda_{\text{ph}}} \int_0^\infty d\omega \frac{\alpha^2(\omega) F(\omega)}{\omega} \ln(\omega) \right],$$

with

$$\lambda_{\text{ph}} = 2 \int_0^\infty d\omega \frac{\alpha^2(\omega) F(\omega)}{\omega} \quad (3)$$

and $\alpha^2(\omega)$ as the electron-phonon interaction function. In a previous work we suggested to use an approach of the form $\alpha^2(\omega) = \delta/\sqrt{\omega}$, with scaling parameter

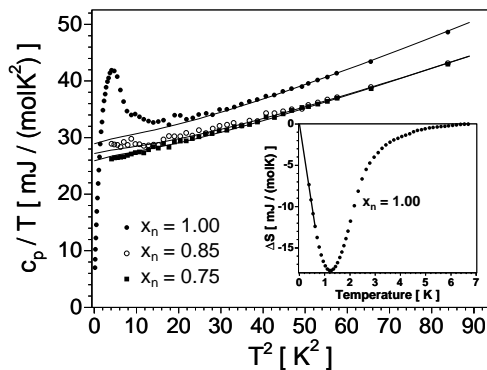


Figure 4: Specific heat of MgC_xNi_3 at low temperatures. Solid lines: fits to the data (see text for details). The anomaly at $T \approx 2.5 \text{ K}$ for sample $x_n = 1.00$ indicates the superconducting transition. Inset: entropy change of the electronic specific heat within the superconducting state for $x_n = 1.00$.

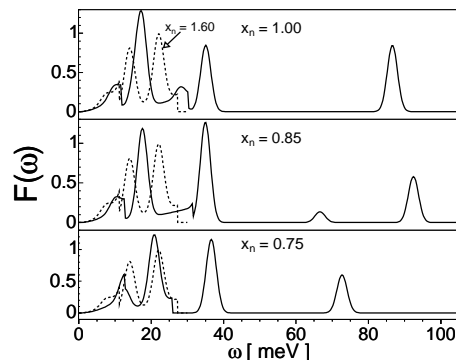


Figure 5: Phonon density of states of MgC_xNi_3 . Dashed lines: result for $x_n = 1.60$.⁶

δ to approximate the electron-phonon interaction function. Within this approach the low-energy phonons are more strongly weighted. Calculating ω_{ln} for the present samples, an increase from $\omega_{\text{ln}} = 154 \text{ K}$ ($x_n = 1.00$) to 162 K ($x_n = 0.85$) and 164 K ($x_n = 0.75$), compared to $\omega_{\text{ln}} = 143 \text{ K}$ for $x_n = 1.60$ is found.⁶ Even by leaving out the carbon-dominated high-energy mode in the calculation, ω_{ln} is still increasing [$\omega_{\text{ln}} = 148 \text{ K}$ ($x_n = 1.00$), $\omega_{\text{ln}} = 154 \text{ K}$ ($x_n = 0.85$), $\omega_{\text{ln}} = 155 \text{ K}$ ($x_n = 0.75$)].

This unambiguously demonstrates that the influence of carbon on the low-energy modes, which are crucial for the observed strong electron-phonon coupling in MgCNi_3 (see Ref. 14) can not be neglected. A similar result was already derived from structural investigations.⁷ In order to stress this point, λ_{ph} was calculated from Eq. (3), using $\delta \approx 4.8$ from Ref. 6. Fig. 6 shows a comparison of λ_{ph} determined by Eq. (1) and Eq. (3), respectively. From the phonon density of states a linear dependence from the effective carbon content x_e is derived (open sym-

Table I: Experimental quantities and electron-boson coupling constants as derived from the electronic specific heat.

		MgC _x Ni ₃			
x_n	[a. u.]	1.60	1.00	0.85	0.75
x_e	[a. u.]	0.967	0.856	0.822	0.796
T_c^{exp}	[K]	6.80	$\sim 2.5^a$	< 2	< 2
γ_N	[mJ/molK ²]	31.4	24.8	23.5	22.7
λ_{ph}		1.84	1.25	1.14	1.06
$\lambda_{\text{sf}}(0)$		0.43	0.38	0.35	0.30

^awith $T_c^{\text{onset}} \approx 6$ K from ac-susceptibility measurements.

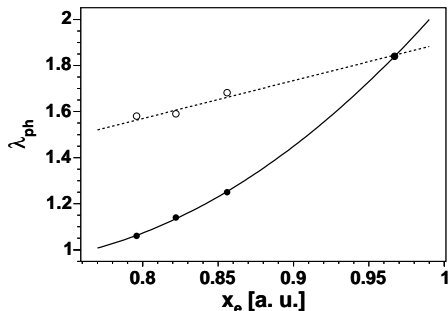


Figure 6: Electron-phonon coupling constant vs. effective carbon content. Filled symbols: determined from Eq. (1). Open symbols: calculated from Eq. (3). The lines are guides to the eye.

bols), which strongly overestimates the non-linear result determined from Eq. (1) (filled symbols). This strongly indicates that carbon-deficiency not only influences the low-energy phonons within the series but also changes

the electron-phonon interaction function $\alpha^2(\omega)$, entering Eq. (3).

The present results clearly point to the importance of carbon for stabilizing the low-energy Ni-dominated phonon modes which are expected to lead to the high electron-phonon coupling in this compound.¹⁴ A similar scenario was established by Johannes and Pickett, who attributed the phonon hardening in carbon-deficient MgCNi₃ and the related carbon-deficient ZnCNi₃ to the low-energy Ni “breathing” mode.¹⁰ It seems unlikely that the observed strong decrease of λ_{ph} is explained by the decreasing lattice parameter only, since pressure experiments show an increase of T_c with increasing pressure.^{15,16} Considering a possible decrease of the EDOS,⁵ one would expect slightly higher values of λ_{ph} . However, considering the well known McMillan formula and the low $T_c \lesssim 2.5$ K of the samples with $x_n \leq 1.00$ this effect seems to be negligible.⁶ The present results may also help to understand recent investigations of the carbon isotope effect performed by Klimczuk and Cava,¹¹ which is much stronger than expected from calculations.^{14,17} Further experimental and theoretical studies of the evolution of the EDOS as well as the PDOS of carbon-deficient and isotope-pure samples and the behavior of the electron-phonon interaction function $\alpha^2(\omega)$ are highly desirable.

Acknowledgments

The DFG (SFB 463) is gratefully acknowledged for financial support. We thank S. V. Shulga for fruitful discussions and the help in fitting the paramagnon contribution.

* Electronic address: waelte@ifw-dresden.de

¹ T. He, Q. Huang, A. P. Ramirez, Y. Wang, K. A. Regan, N. Rogado, M. A. Hayward, M. K. Haas, J. S. Slusky, K. Inumara, H. W. Zandbergen, N. P. Ong, R. J. Cava, *Nature* **411**, 54 (2001).

² H. Rosner, R. Weht, M. D. Johannes, W. E. Pickett, and E. Tosatti, *Phys. Rev. Lett.* **88**, 027001 (2002).

³ D. J. Singh and I. I. Mazin, *Phys. Rev. B* **64**, 140507(R) (2001).

⁴ P. M. Singer, T. Imai, T. He, M. A. Hayward, and R. J. Cava, *Phys. Rev. Lett.* **87**, 257601 (2001).

⁵ L. Shan, K. Xia, Z. Y. Liu, H. H. Wen, Z. A. Ren, G. C. Che, and Z. X. Zhao, *Phys. Rev. B* **68**, 024523 (2003).

⁶ A. Wälte, G. Fuchs, K.-H. Müller, A. Handstein, K. Nenkov, V. N. Narozhnyi, S.-L. Drechsler, S. V. Shulga, L. Schultz, and H. Rosner, *Phys. Rev. B* **70**, 174503 (2004).

⁷ T. G. Amos, Q. Huang, J. W. Lynn, T. He, and R. J. Cava, *Sol. State Comm.* **121**, 73 (2002).

⁸ Z. A. Ren, G. C. Che, S. L. Jia, H. Chen, Y. M. Ni, G. D. Liu, and Z. X. Zhao, *Physica C* **371**, 1 (2002).

⁹ P. J. T. Joseph and P. P. Singh, *cond-mat/0504659*.

¹⁰ M. D. Johannes and W. E. Pickett, *Phys. Rev. B* **70**, 060507(R) (2004).

¹¹ T. Klimczuk and R. J. Cava, *Phys. Rev. B* **70**, 212514 (2004).

¹² J. Rodriguez-Carvajal, Abstracts of the Satellite Meeting on Powder Diffraction of the XV Congress of the IUCr p. 127 (1990), Toulouse, France.

¹³ R. Brun and F. Rademakers, *Nucl. Inst. & Meth. in Phys. Res. A* **389**, 81 (1997), <http://root.cern.ch/>.

¹⁴ A. Y. Ignatov, S. Y. Savrasov, and T. A. Tyson, *Phys. Rev. B* **68**, 220504(R) (2003).

¹⁵ H. D. Yang, S. Mollah, W. L. Huang, P. L. Ho, H. L. Huang, C.-J. Liu, J.-Y. Lin, Y.-L. Zhang, R.-C. Yu, and C.-Q. Jin, *Phys. Rev. B* **68**, 092507 (2003).

¹⁶ G. Garbarino, M. Monteverde, M. Núñez-Regueiro, C. Acha, R. Weht, T. He, K. A. Regan, N. Rogado, M. Hayward, and R. J. Cava, *Physica C* **408-410**, 754 (2004).

¹⁷ O. V. Dolgov, I. I. Mazin, A. A. Golubov, S. Y. Savrasov, and E. G. Maksimov (2005), *cond-mat/0506362v1*.